Biomaterials Science

ROYAL SOCIETY OF CHEMISTRY

PAPER

View Article Online
View Journal | View Issue

Cite this: *Biomater. Sci.*, 2020, **8**, 2611

The electrospinning of a thermo-responsive polymer with peptide conjugates for phenotype support and extracellular matrix production of therapeutically relevant mammalian cells†

F. A. A. Ruiter, ‡[a] L. E. Sidney, [b] K. L. Kiick,[c] J. I. Segal,[d] C. Alexander [a] and F. R. A. J. Rose *[a]

Current cell expansion methods for tissue engineering and regenerative medicine applications rely on the use of enzymatic digestion passaging and 2D platforms. However, this enzymatic treatment significantly reduces cell quality, due to the destruction of important cell-surface proteins. In addition, culture in 2D results in undesired de-differentiation of the cells caused by the lack of 3D similarity to the natural extracellular matrix (ECM) environment. Research has led to the development of thermo-responsive surfaces for the continuous culture of cells. These thermo-responsive materials properties can be used to passage cells from the surface when the cell culture temperature is reduced. Here we report the development of a PLA/thermo-responsive (PDEGMA) blend 3D electrospun fibre-based scaffold to create an enzymatic-free 3D cell culture platform for the expansion of mammalian cells with the desired phenotype for clinical use. Human corneal stromal cells (hCSCs) were used as an exemplar as they have been observed to de-differentiate to an undesirable myo-fibroblastic phenotype when cultured by conventional 2D cell culture methods. Scaffolds were functionalised with a cell adherence peptide sequence GGG-YIGSR by thiol–ene chemistry to improve cell adherence and phenotype support. This was obtained by functionalising the thermo-responsive polymer with a thiol (PDEGMA/PDEGSH) by co-polymerisation. These incorporated thiols react with the norbornene acid functionalised peptide (Nor-GGG-YIGSR) under UV exposure. Presence of the thiol in the scaffold and subsequent peptide attachment on the scaffolds were confirmed by fluorescence labelling, ToF-SIMS and XPS analysis. The biocompatibility of the peptide containing scaffolds was assessed by the adhesion, proliferation and immuno-staining of hCSCs. Significant increase in hCSC adherence and proliferation was observed on the peptide containing scaffolds. Immuno-staining showed maintained expression of the desired phenotypic markers ALDH, CD34 and CD105, while showing no or low expression of the undesired phenotype marker α-SMA. This desired expression was observed to be maintained after thermo-responsive passaging and higher when cells were cultured on PLA scaffolds with 10 wt% PDEGMA/4 mol% PDEGS-Nor-GGG-YIGSR. This paper describes the fabrication and application of a first generation, biocompatible peptide conjugated thermo-responsive fibrous scaffold. The ease of fabrication, successful adherence and expansion of a therapeutically relevant cell type makes these scaffolds a promising new class of materials for the application of cell culture expansion platforms in the biomaterials and tissue engineering field.

Received 19th December 2019,
Accepted 22nd January 2020

DOI: 10.1039/c9bm01965k

rsc.li/biomaterials-science

[a]*School of Pharmacy, University of Nottingham, UK.*
E-mail: f.ruiter@maastrichtuniversity.nl, felicity.rose@nottingham.ac.uk, cameron.alexander@nottingham.ac.uk
[b]*Division of Clinical Neuroscience, University of Nottingham, UK.*
E-mail: laura.sidney@nottingham.sc.uk
[c]*Department of Material Science and Engineering, University of Delaware, USA.*
E-mail: kiick@udel.edu
[d]*Faculty of Engineering, University of Nottingham, UK.*
E-mail: joel.segal@nottingham.ac.uk

†Electronic supplementary information (ESI) available. See DOI: 10.1039/c9bm01965k

‡FAA Ruiter is now working at Maastricht University in the MERLN institute.

Introduction

Current methods of adherent mammalian cell expansion for tissue engineering and regenerative medicine applications rely usually on the use of 2D culture platforms, foetal bovine serum containing media, and enzymatic digestion for cell recovery. However, 2D culture of primary cells can result in undesired de-differentiation,[1–3] due to the lack of similarities to the natural extracellular matrix (ECM) environment, and enzyme passaging can significantly reduce cell quality,[4–6] as a

result of the destruction of important cell-surface proteins. In recent years, thermo-responsive surfaces[7,8] have been used as supports for mammalian cell culture, as their changes in physicochemical properties at upper or lower critical solution temperatures (UCST, LCST) can facilitate cell detachment without the need for enzymatic passaging.[9–13] PNIPAM is the most commonly used thermo-responsive polymer, however, the presence of strong hydrogen bond donors and hydrogen acceptors in its structure can lead to inter- and intra-chain association entanglement.[14] By comparison, PEG-based polymers have a reversible phase transition that occurs without chain entanglement. These polymers are therefore widely used in the drug delivery and biological fields.[7,10,15–17] Although, the polymer phase transitions result in measurable "hydrophilic-to-hydrophobic" behaviour changes, these differences are often only moderate in terms of their effects on cell adhesion. Accordingly, there is a need to generate materials, which provide selective functionality for specific cells to attach, while retaining their ability to release cells *via* a mild temperature change at the end of the cell culture and expansion period. We therefore selected a PEG-based polymer that is amenable to functionalisation without loss of the thermo-responsive behaviour, an attribute that has widely been shown in the literature.[15,16,18–20]

Here we report the development of a new cell adhesion peptide (GGG-YIGSR) functionalised thermo-responsive fibre-scaffold based on co-electrospun poly(DL-lactide) (PLA) and poly(di(ethylene glycol) methyl ether methacrylate)-*co*-poly(di(ethylene-glycol) carboxylate ester ethyl thiol) (PDEGMA/SH, Fig. 1A) for enzyme-free 3D mammalian cell culture. We have exemplified this concept *via* the growth and recovery of human corneal stromal cells (hCSCs) in non-serum containing media. These cells were chosen as hCSCs display a well characterised phenotypic change during conventional *in vitro* culture from a keratocyte phenotype (quiescent, $CD34^+$, $ALDH^+$) to a mesenchymal stem cell/fibroblast/myofibroblast phenotype (proliferative, $CD105^+$, $\alpha\text{-SMA}^+$).[21] The laminin sequence YIGSR was selected for this study as previous literature has shown that interaction with this peptide sequence supports hCSCs attachment and the maintenance of a quiescent keratocyte phenotype.[22]

Co-spinning PLA with thermo-responsive polymers of PDEGMA and a side-chain thiol-functionalised PDEGSH generated fibrous scaffolds with 'click' handles for peptide coupling. The subsequent conjugation chemistries were carried out by reacting norbornene-fuctionalised peptides (Nor-GGG-YIGSR, Fig. 1C) with the side-chain thiols *via* a UV-mediated thiol–ene reaction (Fig. 1B). Attachment of the peptides on the scaffolds was confirmed by fluorescence labelling, ToF-SIMS and XPS analysis. The resulting bioconjugate scaffolds were assessed for their ability to support hCSCs culture by cell adhesion, proliferation and immunocytochemistry assays. The phenotypic profiling of hCSCs after thermo-responsive passaging was evaluated by flow cytometry analysis of key cell surface markers. The combined assay data indicated that the expansion of hCSCs could be conducted with high yield and retention of a therapeutically desirable phenotype without using expensive and potentially cell-damaging enzymatic methods. The ability to culture, expand and recover therapeutically relevant cell types makes these scaffolds a promising new class of materials for application in many areas of regenerative medicine, where cells are destined for the clinic.

Experimental

Polymer and peptide synthesis

Materials. Hexane, DMF, Fmoc deprotection agent piperazine, activator *N*,*N*′-diisopropylcarbodiimide (DIC), and activator base Oxyma were purchased from Fisher Scientific (Pittsburgh, PA, USA). Fmoc-alanine, Fmoc-glysine, Fmocisoleucine, Fmoc-valine, Fmoc-tyrosin(*t*-butyl), Fmoc-arginine(Boc), Fmoc-lysine(Boc), and Fmoc-serine(*t*-butyl) were purchased from ChemPep, USA. All other materials were purchased from Sigma-Aldrich, Switzerland.

General process of synthesis of poly(di(ethylene glycol) methyl ether methacrylate-*co*-poly(di(ethylene-glycol) vinyl ether (PDEGMA/OH). Di(ethylene glycol) methyl ether methacrylate and di(ethylene glycol) vinyl ether in different ratios, 2-butanone, 1-dodecanethiol and recrystallised AIBN were added in a dry 50 ml round bottom flask, degassed for 25 min with N_2, closed and heated to 60 °C for 1 h. The mixture was cooled to room temperature (rt) and precipitated in hexane (500 mL), resuspended in 2-butanone and precipitated in hexane for an additional three times. The resultant polymer was dried overnight and identified by 1D, 2D ^{1}H-NMR, C^{13}-NMR and FT-IR (see ESI†).

General process of synthesis of poly(di(ethylene-glycol) methyl ether methacrylate-*co*-poly(di(ethylene-glycol) thiol (PDEGMA/SH). PDEGMA/OH (4.4 mmol), 200 ml toluene, 3-mercaptopropanoic acid (2.2 mmol), *p*-TSA (1.76 mmol) and DTT (2.2 mmol) were added in a dry round bottom flask and refluxed for 48 hours at 135 °C with a Dean stark trap. Toluene was removed by rotary evaporation and the product was precipitated in cold ether for three times. The resultant polymer was dried under vacuum and identified by 1D, 2D ^{1}H-NMR, C^{13}-NMR and FT-IR (see ESI†).

General process of synthesis of norbornene functionalised peptides

Norbornene acid (Nor) functionalised peptide Nor-GGG-YIGSR was synthesised on a Rink Amide Resin (ChemPep, Wellington, FL) with a Liberty Blue™ peptide synthesizer (CEM Corporation, United Kingdom). Amino coupling cycles were as followed: Fmoc deprotection, 4× washing, coupling, coupling, 2× washing. The N-terminus of each peptide was functionalised by a norbornene acid end group using the same coupling cycle. These norbornene functionalised peptide were cleaved off the resin in a strong acid 95% trifluoracetic acid (TFA), 2.5% deionised H_2O, and 2.5% triisopropylsilane under shaking for 4 h. Cleaved resin was filtered off, TFA was evaporated until 20% of the volume was left, and peptide were preci-

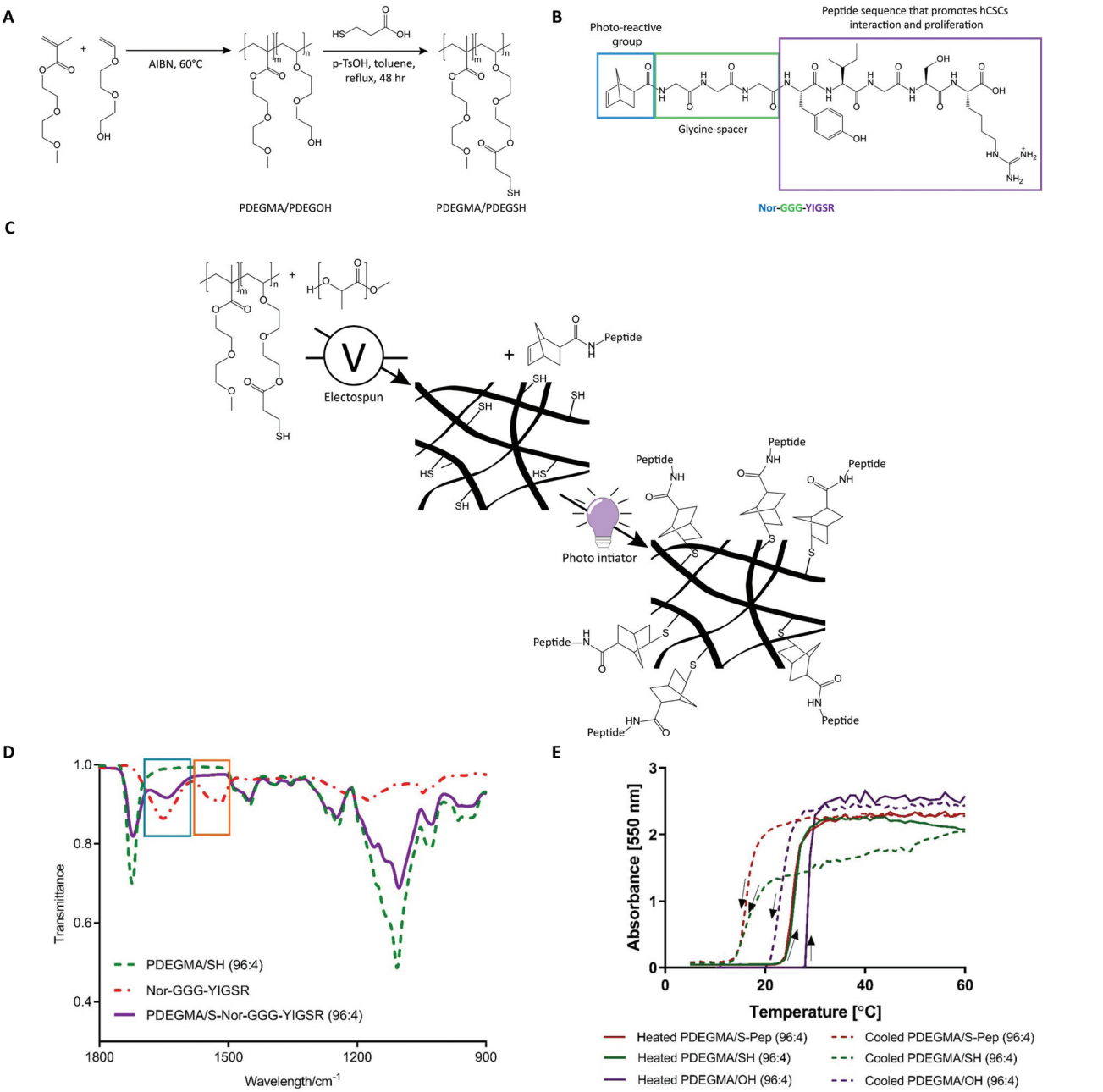

Fig. 1 Schematics of (A) the PDEGMA/PDEGSH (PDEGMA/SH) synthesis, (B) the formation of polymer–peptide derivative electrospun scaffolds, (C) the chemical structure of the synthesised Nor-GGG-YIGSR peptide sequence. Nor (blue block) is the norbornene acid photo-reactive group, GGG (green block) is used as a spacer and YIGSR (purple block) sequence previously identified to promote hCSCs proliferation. (D) FT-IR spectra from pure Nor-GGG-YIGSR (red), PDEGMA/SH (green) and peptide functionalised PDEGMA/PDEGS-Pep by photo-initiated thiol–ene chemistry (purple). The double bond from the norbornene acid disappeared and the amino groups of the peptide appeared on the FT-IR of the functionalised polymer–peptide. (E) Cloud point hysteresis of PDEGMA, PDEGMA/PDEGOH (PDEGMA/OH), PDEGMA/PDEGSH (PDEGMA/SH) and PDEGMA/PDEGS-Nor-GGG-YIGSR (PDEGMA/S-Pep) in water (2 mg ml^{-1}). Arrows up are the heating spectra and arrows down are the cooling spectra. Transition temperature (T_t) shift down when polymer cools down. This is due to the aggregation of the polymer, which takes time to break up. PDEGMA/OH T_t is slightly higher in temperature due to the additional hydrophilic group OH. PDEGMA/SH polymer shows an earlier T_t change than the PDEGMA and PDEGMA/OH polymers as well as a slow steady slope when cooled.

pitated three times in cold ethyl. Sample was re-suspended in 80% water and 20% acetonitrile (ACN), frozen in liquid nitrogen, and lyophilised. Dried peptide was then reconstituted in the same water ACN acetic acid ratio and purified by preparative-scale reverse-phase high performance liquid chromatography (RP-HPLC) using a Waters Xbridge BEH130 Prep C-18 column. The mobile phase comprised gradients of degassed, deionised water with 0.1% TFA and ACN with 0.1% TFA, at a

flow rate of 21 ml min^{-1}. The peptide was detected by UV absorbance at 214 nm, fractions were collected and lyophilised. Molecular weight of the purified peptide was verified by electrospray ionization mass spectrometry (ESI-MS, AutospecQ, VG Analytical, Manchester, UK).

Blend electrospun scaffold fabrication and polymer–peptide conjugation

Production of blended PLA with PDEGMA/SH electrospun scaffolds. Electrospun solutions were prepared in Ac : DMF (1 : 1) with PLA (25% w/v) and PDEGMA/SH (10 wt%) at rt by stirring. Obtained scaffolds were fabricated using a Climate Control EC-CLI platform with rotating target collector EM RTC electrospin unit (IME Technologies, the Netherlands, Geldrop) with a 0.8 mm internal diameter (21 gauge) flat tip needle. The conducting surface was reduced to a width of 5 cm (appr. 100 cm^2 surface area) by covering either side of the rotating mandrel (7.5 cm diameter) with parafilm. The climate control system was started 30 min before the run to obtain constant temperature and humidity of 20 °C and 44% respectively. A total volume of 2 ml polymer solution per run was used for each scaffold batch. Applied voltage, needle-to-collection mandrel distance and flow rate were set to 19 kV, 17.5 cm and 0.5 ml h^{-1} respectively.

Thiol–ene conjugation of PDEGMA/S-Nor-GGG-YIGSR or electrospun scaffolds PLA and PDEGMA/S-Nor-GGG-YIGSR blend. PDEGMA/SH polymer (1 eq.) was dissolved in PBS to a concentration of 1 mg mL^{-1}, 10 eq. TCEP was added and left on a shaker in a cold room (8 °C). Nor-GGG-YIGSR (1 eq.) was dissolve in DMSO and added to the polymer TCEP solution. 55 μL LAP solution of 13.4 mg mL^{-1} in PBS was added and sample was placed under a 365 nm mercury spot UV lamp (Blak-Ray(r) B-100 AP high intensity UV lamp, uUVP) at a strength of 6 mW cm^{-2} in an ice. Samples were UV exposed for 15 min and a small sample was taken every 5 min to observe the reaction ratio of the thiol–ene click reaction. Resultant product was precipitated by warming, resuspended in cold water and precipitated for three times. Product was dried overnight and characterised by the Ellman's assay and IR measurements. In case of the electrospun scaffolds, the scaffold was submerged in 1 mL PBS (5 mM EDTA, 7.4 pH), 10 eq. TCEP was added and shaken for 30 min in a cold room (8 °C). 10 eq. Nor-GGG-YIGSR and 55 μL LAP solution was added. This was exposed to 365 UV at a strength of 6 mW cm^{-2} for 90 seconds over ice. Scaffolds were washed with PBS before cell seeding.

Electrospun scaffold characterisation

Scanning electron microscope (SEM). For each obtained scaffold a 1 × 1 cm sample was cut out of the centre, mounted on a pin stubs (12.5 mm) with carbon tabs (12 mm) and gold sputter coated for 300 s at 25 mA (EM SCD005, Leica Microsystems). All scaffolds were analysed by SEM (JSM-6060LV, Jeol Ltd Japan) at ×1000, ×2000, and ×5000 magnifications (mag.) with six different fields of view captured for each scaffold.

Fibre diameters and standard deviation measurements. Fibre diameter measurements were performed with ImageJ 1.48v software, six SEM images were taken at ×5000 mag. with 20 fibre measurements per image (120 in total). Beads were included in the measurements and measured on the widest point of the bead. Mean fibre diameter and standard deviation of the measurements were calculated using GraphPad Prism software 7.01 software.

Time-of-flight secondary ion mass spectrometry (ToF-SIMS). Scaffolds were attached to a glass slide by double-sided tape, put into the ToF-SIMS and set under vacuum the night before measurement to obtain a stable vacuum. Negative and positive spectra were collected using an ION TOF, ToF-SIMS IV instrument (Münster, Germany) equipped, with a bismuth liquid metal ion gun (LMIG). A voltage of 25 kV and Bi^{3+} primary ion source were used. The beam was directed at a 45° angle to the sample with a beam spot of 1–2 μm in the high current bunched mode. Three different points of the scaffolds of interest of a surface area of 500 by 500 μm were taken with 256 × 256 pixels, 15 scans (1 shot per pixel). Spectra obtained were analysed and relevant peaks identified by IONTOF GmbH SurfaceLab 6 Software, Germany. Spectra were normalised to total ion count and calibrated with m/z = 1 (H^+), 15 (CH_3^+), 31 (CH_3O^+), 55 ($C_3H_3O^+$), 57 ($C_3H_5O^+$) and 99 ($C_5H_7O_2^+$) for positive spectra and m/z = 1 (H^-), 12 (C^-), 13 (CH_2^-), 14 (CH_3^-) and 15 (CH_4^-) for negative spectra.

X-Ray photoelectron spectrometry (XPS). Samples (0.5 × 0.5 cm cuts) were mounted onto XPS sample stubs and pinned with a copper bar. All XPS analysis were carried out using a Kratos Axis Ultra spectrometer using a mono-chromated aluminium X-ray gun, with a charge-compensating electron flood. Elemental quantification was achieved using CASA software. A linear background was applied to the C 1s high resolution peaks and synthetic Gaussian/Lorentzian peak shapes used to fit the peak components.

Cell culture

Materials. DMEM, trypsin, PBS, 2% gelatin stock, antiboitic–antimycotic (AB/AM) buffer were purchased from Sigma-Aldrich Co Ltd, Switzerland. Trypan Blue Solution (0.4%) was purchased from Thermo Fischer Scientific, UK. Foetal bovine serum (FBS), alamarBlue, TrypLE dissociation reagent, DMEM/F-12 + Glutamax, KnockOut serum replacement (KSR), FGF-basic (bFGF), MEM non-essential amino acids (NEAA) were purchased from Gibco Life Technologies, UK. Human leukaemia inhibitory factor (hLIF) was purchased from Cell Signalling Technologies, the Netherlands.

0.1% (v/v) gelatin coating of 2D cell culture surfaces. T75 and 24 well plates were coated with 0.1% (v/v) gelatin in PBS to improve cell attachment. 0.1% (v/v) gelatin in PBS was made up form stock solution (1% (v/v) gelatin), sterilised through a 0.2 μm filter. 200 ml or 3 ml, 24 well or T75 flask respectively was added, agitated and incubated for 2 h at 37 °C. Excess gelatin solution was removed before cell seeding. Coated T75 flasks were kept in 3 mL PBS in the fridge at 4 °C for up to a week.

hCSCs isolation. Tissue from human donors was used in accordance with the tenets of the declaration of Helsinki, following consent obtained from the donors and/or their relatives. Corneoscleral rims were obtained under an MTA from Nottingham University Hospitals Trust and all work was performed in accordance with the Human Tissue Authority. Corneoscleral rims arrived fully anonymised, thus age, gender and health status are unknown. Excess sclera was removed, and the corneal epithelium and endothelium were gently detached by scraping, resulting in the remaining stromal tissue. This was divided into small pieces and digested in 1 mg mL^{-1} collagenase Type IA (Sigma Aldrich) for 7 h under agitation at 37 °C. The digest solution was filtered through a 40 μm cell strainer, centrifuged, resuspended in culture media (see below), cultured and cryo-preserved at passage number 2.[23,24]

hCSCs cell culture and passaging. hCSCs were cultured stem cell medium (SCM; DMEM/F11 + GlutaMAX with 20 w/v% KSR, 0.04 w/v% bFGF, 0.01 w/v% hLIF, 0.2 w/v% AB/AM and 1 w/v% MEM non-essential amino acids) in T75 flasks at 40 000 cells per cm^2 in SCM and incubated at 37 °C, 5% CO_2. Media was changed every 2–3 days. Passaging was performed at 80% confluency (7–9 days culture) using TripLE. Cells were used experimentally at passage 3.

Scaffold preparation and sterilisation. Electrospun scaffolds were cut into 1.5 cm by 1.5 cm squares which were fixed in CellCROWN™ inserts (no filter, non-sterile, Z742380-12EA), resulting in a scaffold surface area of 0.79 cm^2. The fixed scaffold in the inserts were transferred to a non-tissue culture plastic 24 well plate, sterilised for 10 min under UV light at 800 energy level, incubated for 2 h at 37 °C in 1 mL of DMEM containing 10 w/v% AB/AM (100 units per mL penicillin, 100 μg mL^{-1} streptomycin) and washed with PBS (3 × 1 mL).

Cell seeding on electrospun scaffolds. Cells were seeded onto the scaffolds (1 ml per well, 60 000 cells per mL) in SCM and incubated at 37 °C, 2% CO_2. Media was changed every 2 to 3 days culture.

Proliferation study using the cell viability assay, Alamar blue. Scaffolds were rinsed with warm Hank's balanced salt solution (HBSS, 37 °C) for 3 times. Alamar blue working solution (500 μL; 10 w/v% Alamar blue in DMEM) was added to the scaffolds. Cells adherent to tissue culture plastic (24 well, triplicate) served as a positive control and unseeded scaffolds for a negative control. The Alamar blue and scaffolds were incubated for 90 min at 37 °C and fluorescence intensity of 100 μl aliquots were analysed using a plate reader (TECAN, infinite R M200, Männedrof, Switzerland at excitation wavelength and bandwidth of 560 nm; 9 nm, emission wavelength and bandwidth of 590 nm; 20 nm, number of flashes 25, integration time 20 s and a gain of 87). Number of cells were calculated with the use of a calibration curve of known hCSC number (see Fig. S11†) and divided by the surface area of the scaffolds or of a single well in a 24 well plate in case of the TCPS control to obtain the number of cells per cm^2. Alamar blue assays were performed at day 0, 2, 5, 7 and 9 of culture. In case of day 0, the cells were allowed to attach after seeding for 6 h. Samples were assayed in-triplicate to be statistically reliable.

Cell immunocytochemistry

Materials. *para*-Formaldehyde (pFA), bovine serum albumin (BSA), glycine, Triton X-100, Donkey serum were purchased from Sigma-Aldrich Co Ltd, Switzerland. 4′,6-Diamidino-2-phenylindole (DAPI) was purchased from Santa Cruz Biotechnology. Alexa-Flour 488-conjugated phalloidin was purchased from New England Biolabs. Antibodies details can be found in Table S1.†

Fixing hCSCs for immuno-staining. Media was removed at day 9 of cell culture, scaffolds was rinsed with PBS, 1 ml 2 w/v% pFA per scaffolds was added and incubated for 10 min at rt. Subsequently, the scaffolds with fixed cells were washed with PBS for 3 times.

Immunocytochemistry of fixed hCSCs on electrospun scaffolds. To observe cell morphology, phenotype expression and ECM expression of the hCSCs on the different electrospun scaffolds four different immuno-staining combinations were selected, see Table S2† (see Table S1† for primary and secondary antibodies used).

Scaffolds were moved from the Cell CROWN™ and placed in a new non-treated 24 well plate, 200 μL permeabilisation buffer (0.1% Triton-X100 in PBS) was added per scaffold for immunostaining combinations B, C and D and incubated for 10 min at rt. Permeabilisation buffer was removed and scaffolds were washed with PBS (3×). All washing steps lasting 5 min each. 200 μL of blocking buffer (3% Donkey serum in wash buffer; 1% BSA, 0.3 M glycine in PBS) was added per scaffold for all immuno-staining combinations and incubated for 1 h at rt.

Subsequently, 200 μL of primary antibody solution was added according to the immuno-staining combination per scaffold at the required dilution factor prepared in wash buffer (1% BSA, 0.3 M glycine in PBS; see Table S2†). Samples were incubated at 4 °C for 16 h. Negative controls were incubated in wash buffer only. The primary antibody solutions were removed, scaffolds were rinsed with wash buffer (3×). Secondary antibodies (200 μL) were added per scaffold, including negative controls and incubated for 1 h at rt in the dark (covered in foil). Subsequently, washed with PBS (3×). Scaffolds of combination C were incubated for 20 min in the dark in 200 μL actin solution (see dilution, Table S2†) and washed with PBS (3×).

All nuclei were stained with DAPI. DAPI (200 μL) was added per scaffold and incubated for 10 min at rt in the dark, washed with PBS (3×) and stored in PBS at 4 °C.

Confocal microscopy imaging. Scaffolds were removed from the PBS and placed on a coverslip. Images were measured with a 4× and 20× lens of the upright fluorescence microscope (BX51, Olympus) with images captured with a black and white camera (XM-10, Olympus) and Cell^F software (Olympus). Wavelength of 405 nm, 488 nm and 566 nm for DAPI, CD34/ALDH/actin/collagen I and CD105/α-SMA/Vimentin/Lumican, respectively were used.

hCSCs thermo-responsive detachment studies and phenotype expression after detachment by flow cytometry

hCSCs thermo-responsive detachment studies. Scaffolds were removed from the Cell CROWN™ and placed in a new non-tissue culture treated 24 well plate and submerged in 1 mL SCM. This well plate was incubated for 30 min at 4 °C. Scaffolds were vigorously agitated in the SCM media. Subsequently, the SCM with detached cells were moved into a new tissue-culture treated 24 well plate and incubated for 6 h before performing the Alamar blue viability assay. The remaining scaffolds were left in the well plate and new SCM 1 mL was added and incubated for 6 h and subsequently the Alamar blue viability assay was performed, to see if any cells were remaining on the scaffold after detachment.

Percentage of cells detached was calculated by subtracting the number of cells on the scaffold left after passaging with the initial number of cells before passaging. This number was then defined by initial number of cells and multiplied by 100.

Immunostaining of suspended cells for flow cytometry. hCSCs were thermo-responsively detached from the scaffolds, re-suspended in 2 w/v% pFA and fixed for 30 min, centrifuged (5 min at 500*g*) and re-suspended in PBS. Samples were stained in combinations A and B (see Table S2†), washed between every step by centrifugation (3× for 5 min at 300*g* each washing step). CD34, CD105, ALDH and α-SMA on their own were used as positive control, while, the negative control was incubation with the secondary antibody alone (without the primary antibodies).

Flow cytometry. Flow cytometry was performed (MoFLo Astrios™ Beckman Coulter, USA) to quantify cell populations expressing certain markers of interest. Samples were agitated before analysis to assure single cells were in suspension. Data obtained were analysed by Kaluza Analysis software and obtained X-means and Y-means were analysed with two-way ANOVA using GraphPad Prism 7.01 software.

Characterisation techniques

1D 1-hydrogen and carbon-13 NMR analysis (^{1}H-NMR and C^{13}-NMR). ^{1}H-NMR and C^{13}-NMR spectra were recorded on a Bruker Avance III 400 spectrometer at 399.8 MHz (^{1}H) and 100.5 MHz (C^{13}) in deuterium chloroform ($CDCl_3$). MestReNova 11.0 software was used to analyse the obtained spectra. All chemical shifts are reported in part per million (ppm) relative to $CDCl_3$ (7.24 ppm for ^{1}H-NMR and 77.2 ppm for C^{13}-NMR) or tetramethylsolane (TMS).

2D-NMR heteronuclear single-quantum correlation spectroscopy analysis (HQSC). HSQC 2D-NMR spectra was recorded on a Bruker Avance III 400 spectrometer at 399.8 MHz in $CDCl_3$. MestReNova 11.0 software was used to analyse the obtained spectra. All chemical shifts are reported in part per million (ppm) relative to $CDCl_3$ (7.24 ppm for ^{1}H-NMR and 77.2 ppm for C^{13}-NMR).

Gel permeation chromatography (GPC) analysis. Molar masses of the polymers were measured in tetrahydrofuran (THF) eluent. THF samples were measured using a Waters GPC (Milford, MA) with two Water Styragel (HR1 and HR4) columns, a Waters 2695 auto-sample pump and a refractive index (RI) detector (Waters 410). Samples were eluted at 40 °C at a flow rate of 1.0 mL min^{-1}. Calibration was performed using linear poly(methyl methacrylate) (PMMA) standards (Polymer Laboratories) in the molecular weight range 1–1200 kDa. Molecular weights and dispersity values were calculated using Cirrus GPC 3.0. The samples were dissolved in THF in a concentration of 10 mg mL^{-1} and filtered through 0.45 μm filters to remove any big particles and unwanted impurities.

Fourier transform infra-red (FT-IR) analysis. Samples were measured using an Agilent FT-IR spectrometer, Agilent Technologies, UK. Solid samples were put on top of the diamond, pressure was applied and spectra measured.

Measurement of polymer solution cloud points to estimate lower critical solution temperature (LCST). Thermo-responsive polymer solution (1 mL; 2 mg ml^{-1} in dH_2O) was added into an ultraviolet-visible (UV/VIS) cuvette and placed into the UV/VIS equipment. The chamber was cooled to 5 °C before measurement using a Quantum Northwest Peltier-Controlled Cuvette Holder (Quantum Northwest Inc, WA, USA). UV-VIS absorbance was measured by Agilent Technologies Cary 60 UV/VIS (Santa Clara, CA, USA) at 550 nm wavelength while the solution was heated at 60 °C at a rate of 1 °C min^{-1}, incubated at 60 °C for 5 min and cooled to 5 °C at 1 °C min^{-1}. An approximation of the LCST was determined at the solution cloud point temperature when a non-linear increase of the absorbance was observed.

Free thiol confirmation by the Ellman's assay. Cysteine hydrochloride monohydrate standard curve solutions of final concentrations of 0, 0.25, 0.5 to 1.5 mM and Ellman's reaction solution (4 mg in 1 ml reaction buffer (0.1 M sodium phosphate and 1 mM EDTA, pH 8.4) were prepared. Cysteine standard curve solution (250 μL) was added to 2.5 mL reaction buffer and 50 μL Ellman's solution, mixed and incubated for 15 min at rt. UV absorbance was measured by Agilent Technologies Cary 60 UV-Vis (Santa Clara, CA, USA) at 412 nm wavelength. A standard curve was fitted (R_2 = 0.99), with the resulting equation Abs = 1.108 × number of free thiols was used as reference for number of free thiols in the PDEGMA/SH solution samples (see Fig. S8B†). PDEGMA/SH polymer samples of 2 mg mL^{-1} were prepared. 250 μL polymer solution was added to 2.5 mL reaction buffer and 50 μL Ellman's reagent solution, incubated for 15 min at rt, and absorbance measured at 412 nm. Percentage free thiol were calculated by the following equation. Percentage free thiols = (mmol polymer per mmol free thiols) × 100.

Free thiol presents in polymers and blend electrospun scaffolds confirmation by flouresceine-5-maleimide labelling. One drop of 100 mL (4 mg ml^{-1}, PDEGMA/SH polymer in acetone) was dried on a glass slide. The dried polymers on the glass slides or electrospun PLA + PDEGMA/SH blend scaffolds were submerged in 3 mL PBS (5 mM EDTA). 30 μL TCEP solution (0.1 mg ml^{-1}, 10 eq.) and incubated for 30 min at rt. Flouresceine-5-maleimide solution (0.01 mg mL^{-1} in PBS) was

added to the glass slide or scaffolds (1 : 1 ratio, SH : maleimide group), incubated for 30 min at rt and washed with PBS (3×) and imaged under confocal; images where enhanced to observed lower signals on the fibres.

Peptide presence confirmation by ATTO-NHS-ester. Blend electrospun scaffolds were submerged in 3 mL PBS (5 mM EDTA). 30 μL TCEP (0.1 mg ml^{-1}, 10 eq.) was added, incubated for 30 min at rt. 10 eq. Nor-GGG-YIGSR and 55 μL LAP solution was added, exposed to a 365 UV lamp at a strength of 6 mW cm^{-2} for 90 seconds over ice. Scaffolds were washed with deionised water; a stock solution of 0.01 mg mL^{-1} ATTO-NHS-ester was then added to scaffolds (1 : 1 ratio, peptide : ATTO group), incubated for 30 min at rt and washed with PBS (3×) and imaged under confocal; images where enhanced to observed lower signals on the fibres.

Results and discussion

Polymer synthesis

The co-polymers PDEGMA/SH in different ratios (100 : 0, 98 : 2, 97 : 3, 96 : 4, and 90 : 10, PDEGMA to PDEGSH respectively) were synthesised by a two-step route (scheme. Fig. 1A). PDEGMA/PDEGOH polymer was synthesised by free radical synthesis with subsequent thiol functionalisation *via* a condensation reaction to form the PDEGMA/SH product. Structures were confirmed by 2D-NMR analysis (Fig. S1–S18†) with the disappearance of the $C\underline{H}_2OH$ signal (H^1-NMR; 3.7–3.8 ppm, t, 2H and C^{13}-NMR; 61 ppm) and the appearance of the $C\underline{H}_2SH$ peaks (H^1-NMR; 2.9 ppm, t, 2H and C^{13}-NMR; 34 ppm) in the H^1 and C^{13}-NMR of the end product PDEGMA/SH (Fig. S1–18 for NMR and Table S3† for GPC). Percentages of free thiol in the co-polymers were confirmed by the Ellman's assay (Table 1). The phase transition temperatures (T_t) of the polymers were estimated by cloud point measurements (Fig. 1E, S19 and Table S4†). The norbornene functionalised peptide Nor-GGG-YIGSR was synthesised on a rink amide resin, purified by HPLC and its structure verified by electrospray ionisation mass spectrometry (ESI-MS, Fig. S20†). Upon reaction of the peptide with the thiolated polymer, a decrease in percentage of free thiols was observed at increasing UV exposure times (0, 5, 10 and 15 min), with a conversion of 65% after 15 min (Table 1). Fourier-transform infrared (FT-IR) analysis showed the disappearance of the norbornene double bond (1530 cm^{-1}) and the appearance of the amino-groups (1655 cm^{-1}) of the peptide in the case of the reacted peptide-thiol polymer (Fig. 1D). Cloud point measurements of the PDEGMA/S-Nor-GGG-YIGSR derivatised polymer showed transition temperatures (22 °C when heated and <18 °C when cooled, Fig. 1E and Table S4†), as compared with the PDEGMA/SH precursor, confirming retention of thermoresponsive behaviour after peptide-functionalisation.

Electrospun scaffold fabrication and characterisation

The obtained PDEGMA/SH polymers were successfully blend electrospun with PLA into uniform fibres (19 kV, 17.5 cm, 0.5 mL h^{-1} and 25 w/v% PLA and 10 wt% PDEGMA/SH polymer in Ac/DMF) with an average fibre diameter range of 800–1200 nm (Fig. S22 and Table S5,† optimised *via* previous DoE work[25]). XPS analysis and fluorescence labelling confirmed the presence of free thiols (S(2p) peak at 168.9 eV and fluorescein-5-maleimide labelling respectively) and peptide (N(1s) peak at 399.8 eV and ATTO NHS ester labelling respectively) on the surface of the scaffolds (Fig. S22 and Table S6†). The distributions of the free thiols and peptides on the scaffolds surface were investigated further by ToF-SIMS analysis. Mass spectrometry peaks of the ion fragments were identified and confirmed through literature (Table S7†).[26–29] The ion fragment CH_3O^- attributed to the underivatised PDEGMA was present on the surface, and a decrease in peak intensity of CH_3O^- was observed for all the scaffolds containing PDEGMA/SH co-polymer (Fig. 2A). ToF-SIMS peak distribution images indicated that SH groups were in regions corres-

Table 1 Percentage of detected free thiol groups in the synthesised PDEGMA/SH polymers after the condensation reaction. Detection and free thiol group concentration estimation were carried out *via* an Ellman's assay by detecting the absorbance of the Ellman's assay reaction product. % OH = percentage of OH on the starting polymer before thiol functionalisation. $C_{polymer}$ = concentration of polymer in PBS, Abs = absorbance at 412 nm, C_{thiols} = concentration of thiols calculated from standard curve, and conv. = conversion

Percentage of free thiols in co-polymers

% PDEGOH	$C_{polymer}$ [mmol ml^{-1}]	Abs	C_{thiols} [mmol ml^{-1}]	% PDEGSH
2	70×10^{-4}	0.0877	1.2×10^{-4}	1.7
3	70×10^{-4}	0.1249	1.5×10^{-4}	2.2
4	70×10^{-4}	0.2483	2.6×10^{-4}	3.7
10	70×10^{-4}	0.7328	6.8×10^{-4}	9.7

Percentage of free thiols after thiol–ene chemistry

UV_{time} [min]	$C_{polymer}$ [mmol ml^{-1}]	Abs	C_{thiols} [mmol ml^{-1}]	% PDEGSH	% conv.
0	70×10^{-4}	0.2483	2.6×10^{-4}	3.7	0
5	19×10^{-4}	0.0300	6.8×10^{-4}	2.0	46
10	19×10^{-4}	0.0295	6.8×10^{-4}	2.0	46
15	70×10^{-4}	0.0537	0.9×10^{-4}	1.3	65

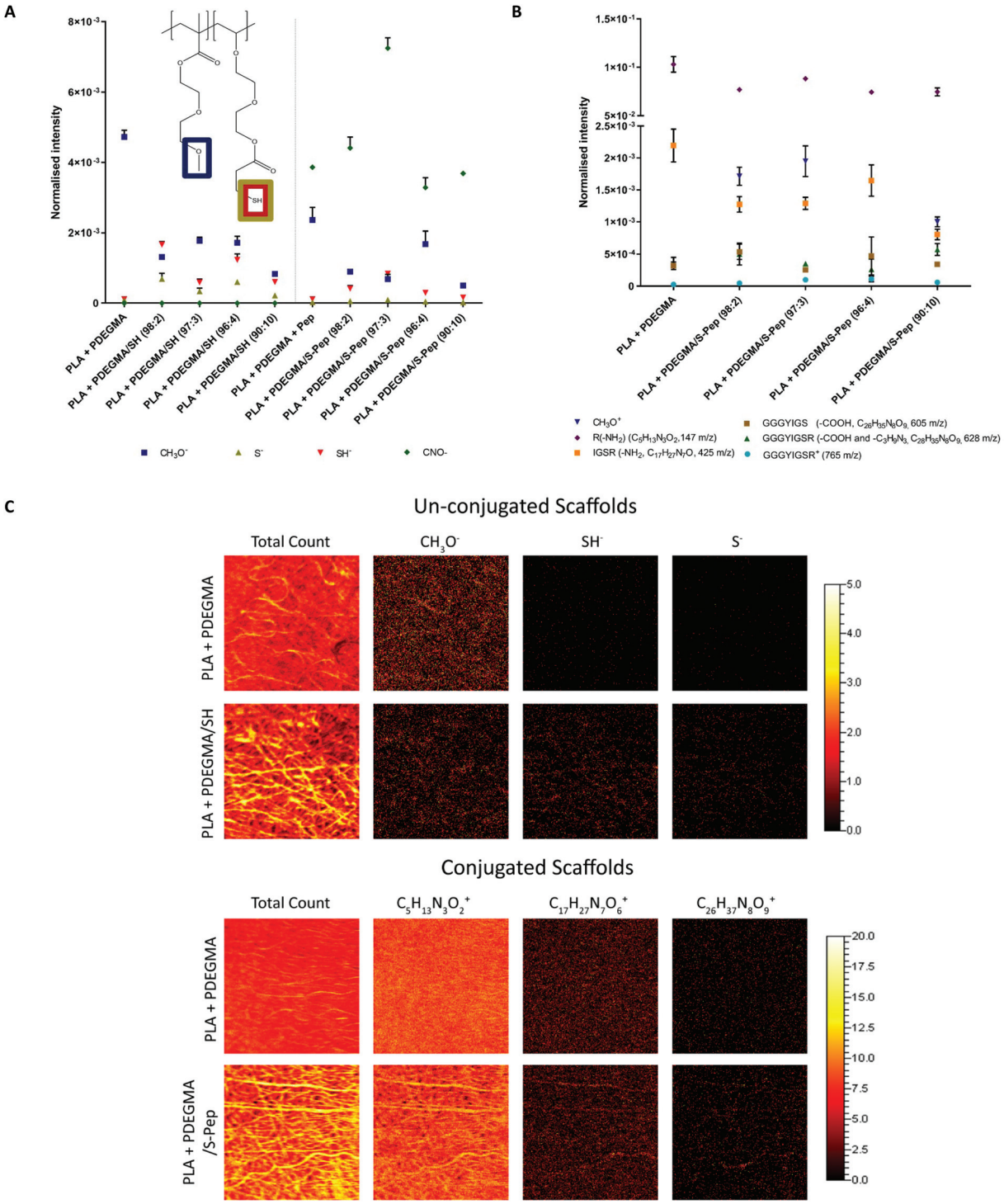

Fig. 2 (A) Total intensity of the ToF-SIMS peaks CH_3O^- (31 *m*/*z*), SH^- (33 *m*/*z*) and S^- (32 *m*/*z*) from the free thiol containing scaffolds. (B) Total intensity of different sequences of the Nor-GGG-YIGSR peptide presences on the scaffold surfaces, (R(–NH_2, 147 *m*/*z*), GSR(–COOOH, 326 *m*/*z*), IGSR(–NH_2, 425 *m*/*z*), GGGYIGS(–COOH, 605 *m*/*z*), GGGYIGSR(–COOH, 628 *m*/*z*) and GGGYIGSR(765 *m*/*z*) (*n* = 3 measurements areas on one scaffold each, data normalised against total count, error bar = SD). (C) ToF-SIMS signal intensity images.

ponding to the fibre positions on the substrate (Fig. 2C and Fig. S22†). An even in S^- and SH^- absorptions were detected for the free thiols on the fibrous surface, confirming an even thiol–ene active distribution sides. A decrease in S^- and SH^- absorptions were detected for the thiol–ene derivatised scaffolds (Fig. 2A). The CNO^- peak of the peptide amino-groups were observed for all scaffolds incubated with peptide (Fig. 2A). Significantly higher intensity was detected for the

scaffold 3 PDEGMA/S-peptide, with a decrease in CNO^- intensity being observed for 4 and 10 PDEGMA/S-peptide (Fig. 2A).

Nor-GGG-YIGSR peptide positive ion fragment signals were identified and were corroborated to literature[30,31] (see fragment structures of identified signals in Fig. S23†). Peptide fragments were detected for all scaffolds, including the PLA + PDEGMA (100 : 0) scaffolds (Fig. 2B). This suggested that non-specific electrostatic binding of the peptide occurred with the surface of the scaffolds. The distribution images of the signal, an even distribution of peptide fragment peaks was observed on the PLA + PDEGMA (100 : 0) scaffold with no thiols present, without a defined fibre morphology (Fig. 2C). However, in case of the peptide-derivatised scaffolds, more defined fibre morphologies were found (see Fig. 2C). This observation indicates the occurrence of specific reaction of the fibre surfaces when free thiols are available, as well as some, albeit low-level, non-specific peptide interaction at the surface of the fibres with no thiols present.

Cell expansion and phenotype support

hCSCs were cultured on the fabricated scaffolds for up to 9 days without loss of scaffold integrity (see protocol ESI section 1†). The media composition of DMEM/F12 with 20% serum replacement, fibroblast growth factor and leukaemia inhibitory factor (SCM) has previously reported to support the keratocyte phenotype of hCSCs[23] and was therefore used in this study. Enhanced proliferation was observed on the scaffolds with an increased content of the laminin mimetic peptide sequence Nor-GGG-YIGSR compared to the PLA + PDEGMA scaffolds (Fig. 3A). Interestingly, significantly higher proliferation was also found on PLA with PDEGMA/SH in the fibres (Fig. 3A). This may be due to presence of free thiols, which promote protein interaction and therefore cell adherence. Morphology staining (actin and vimentin for the cytoskeleton) studies showed clusters of cells on PLA, and PLA with 10 wt% PDEGMA (100 : 0, Fig. 4 and S25–S28†), elongated cell morphologies on PLA with PDEGMA/SH (90 : 10, Fig. S28†), and an increase in a spindle-like morphology of the cells on the peptide derivatised PLA scaffolds with increased PDEGMA/S-Nor-GGG-YIGSR present (Fig. 4 and S26†). The round morphology of the cells on the PLA, and PLA with 10 wt% PDEGMA (100 : 0) scaffolds indicated a limited interaction between the cells and the fibrous scaffold. This in turn suggested that protein deposition of the media was not enhanced when the adhesion peptides were merely adsorbed (as detected by ToF-SIMS analysis) rather than being covalently bound to the fibre surface. The elongated morphologies of cells attached to the thiol-functionalised scaffolds was due most probably to direct cell surface-thiol reactions, for example *via* surface exposed cysteines. This assertion is supported by prior data showing that thiolated surfaces can result in improved ECM protein adsorption and subsequently enhanced cell attachment and proliferation.[32–34] However, significantly more cells exhibiting a spindle-like morphology were observed when the laminin mimetic sequence YIGSR was present (see Fig. 4). Uzunalli *et al.*[22] reported a similar morphology of hCSCs when cultured on YIGSR-containing nanofibres compared to fibronectin-mimetic RGD-peptide nanofibres, as well as increased proliferation, supporting the findings reported here.

Immuno-staining of the hCSCs showed the quiescent keratocyte phenotypic markers CD34 and ALDH, and mesenchymal stem cell (MSC) expression of CD105 on all the different scaffolds (see Fig. 4 and Fig. S26 and 29†). In addition, the expression of myofibroblast marker α-SMA was found when cells were cultured on the PLA and PLA with 10 wt% PDEGMA (100 : 0) scaffolds, and a very low expression of α-SMA was also observed when cells were cultured on the PLA fibres with 10 wt% PDEGMA/SH (90 : 10, Fig. S26 and 29†). This indicates that although the scaffolds with free thiols available do support cell adherence and proliferation as observed in Fig. 3A, α-SMA was still expressed indicating the expression of

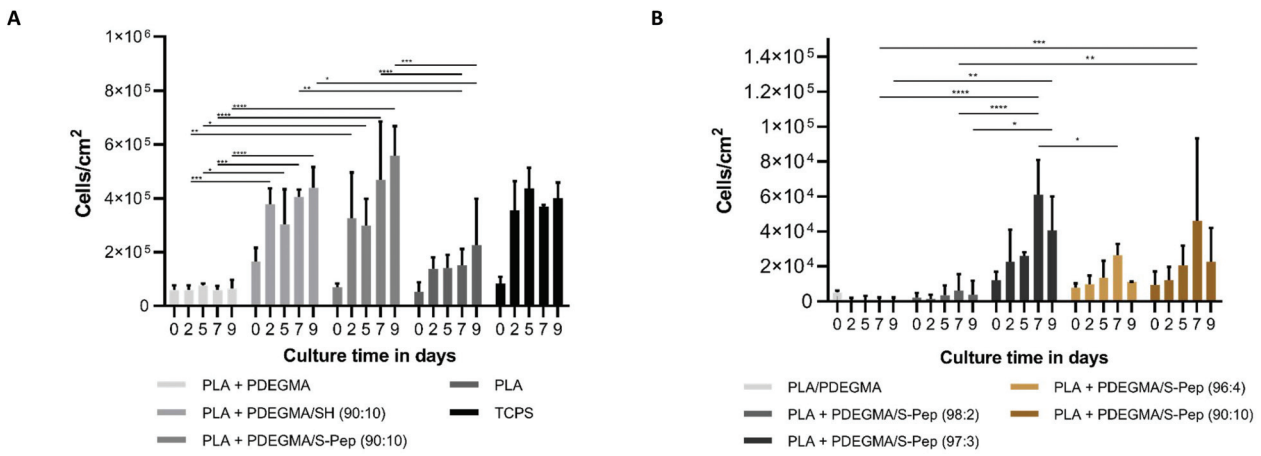

Fig. 3 (A) Cell proliferation in cells per cm^2 of the scaffold different scaffolds types compared to control TCPS over 9 days of culture. (B) Cell proliferation in cells per cm^2 of the peptide derivatised scaffolds with different concentration of peptide attached over 9 days of culture (n = 3 scaffolds, two-way ANOVA, * = <0.05, ** = <0.01, *** = <0.001 and **** = <0.0001, error bars = SD).

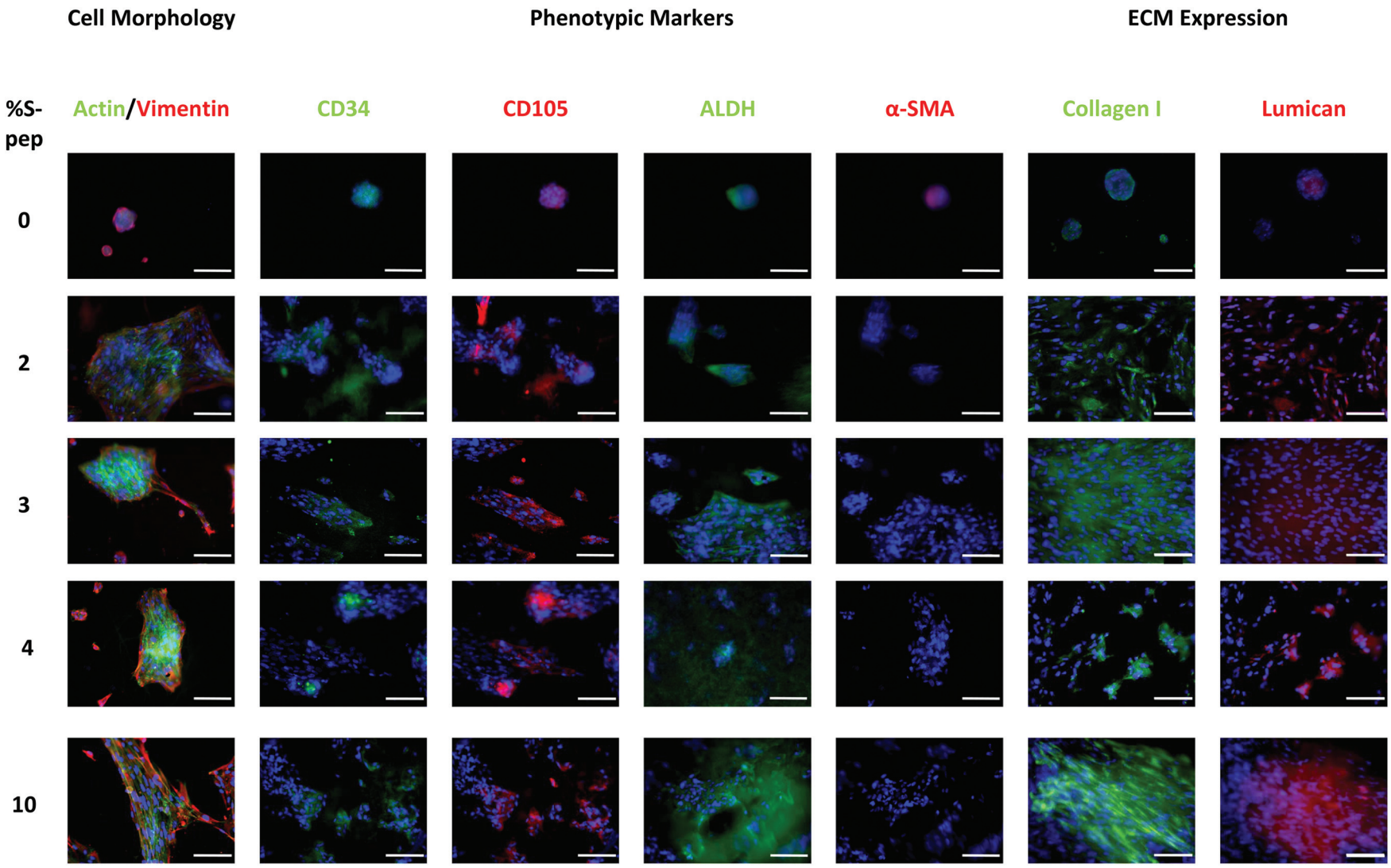

Fig. 4 Immuno-staining to observe hCSC morphology, phenotype expression and ECM expression when cultured on the peptide derivatised PDEGMA/PDEGS-Pep scaffolds at different percentage of peptide. Nuclei are stained with DAPI. Images are enhanced to achieve higher resolution images and separated channel images can be found in ESI Fig. S25–27.† Scale bars correspond to 100 μm.

a myofibroblast phenotype. On the other hand, no α-SMA expression was detected when cells were cultured on any of the PLA fibres functionalised with 10 wt% PDEGMA/S-Nor-GGG-YIGSR (90 : 10). These data confirmed that the peptide supported the quiescent keratocyte phenotype and suppressed de-differentiation of the keratocytes to their activated myofibroblast phenotype.

ECM expression was investigated to confirm the hypotheses that the free thiol group-containing scaffold supported ECM expression and adsorption and hence cell adhesion and proliferation as observed in Fig. S28.† Collagen I expression was observed throughout all the scaffold types (Fig. 4 and S27†), however, this protein increased in abundance and was more evenly distributed on the peptide containing scaffolds (Fig. 4 and S27†). While, collagen I expression was observed near to the clusters of cells on the PLA + PDGEMA (100 : 0) scaffold with absorbed peptide only (Fig. 4 and S27†). These results confirmed that PDEGMA/S-Nor-GGG-YIGSR peptide functionalisation on the scaffold led to an increased expression of collagen I.

Stromal keratocytes express the keratan sulphate proteoglycan, lumican, a corneal transparency factor in a normal undamaged cornea.[32,33] Lumican interacts with collagen fibrils to maintain spacing and transparency in a healthy cornea.[34] Production is significantly reduced during wound healing and phenotypic change to a fibroblast morphology, and thus the presence of lumican can be considered a marker of the quiescent phenotype of hCSCs. As apparent from Fig. 4, lumican expression was found on the scaffolds with peptide present; including the PLA + PDEGMA (100 : 0) scaffolds with non-specific bound peptide. No lumican was present on the scaffold with free thiols, without peptide present (see Fig. S27†). This indicates that the presence of peptide at the surface of the fibres supported ECM expression, while free thiols at the surface do not. However, myofibroblast differentiation and clusters of cells were still observed on the PLA + PDEGMA (100 : 0) scaffolds, suggesting that the non-specifically bound peptide did not support strong cell interactions with the scaffold surface. It was observed that cells spread out across the surfaces only when the peptide was covalently bound to the fibres. Increased lumican expression was detected for the peptide bound scaffolds with 3, 4 and 10 mol% PDEGMA/S-peptide attached, providing support for assertion (Fig. 4). As the derivatised scaffolds with the Nor-GGG-YIGSR peptide were observed to promote the desired quiescent phenotype, spindle-like morphology and ECM expression, the cellular responses on the surfaces with different percentages of peptides attached were investigated. After 9 days cell culture, significantly higher proliferation was observed for 3 and 10% peptide-derivatised scaffolds (97 : 3 and 90 : 10, Fig. 3B). The expression of the quiescent keratocyte phenotype CD34 and ALDH markers were detected for all different concentrations of peptide (Fig. 4). A significantly increased expression of ALDH was observed for the 3 mol% peptide scaffold. As ALDH expression plays an important role in the maintenance of corneal transparency, this indicated a desirable response of the cells in term of their culture on the derivatised fibres. In addition, CD105 MSC marker expression was found on all scaffolds, suggestive of a partial loss of the differentiated quiescent phenotype to a more stem cell-like phenotype.[24] Myofibroblastic α-SMA expression was observed for those cells cultured on scaffolds containing 2 mol% peptide (98 : 2, PDEGMA/S-pep) and on the 0% control (100 : 0), indicating a threshold of peptide content needed to avoid myofibroblast activation. Peptide concentrations of 2 mol% were too low to support the quiescent phenotype and resulted in a myo-fibroblastic change, while cells cultured on scaffolds containing 3, 4 and 10 mol% peptide generated no α-SMA expression. The previously rounded and cluster cell morphology was observed on the scaffolds containing 0 and 2 mol% peptide concentrations, while a more fusiform morphology was observed when cultured on scaffolds with peptide-concentrations 3, 4 or 10 mol% (Fig. 4). Moreover, lumican ECM expression was detected when cells were cultured on scaffolds with higher percentages of peptide on the surface (3, 4, and 10 mol%). It can therefore be concluded that scaffold fibres with more than 2 mol% of Nor-GGG-YIGSR covalently bound to their surfaces significantly improved hCSCs attachment, proliferation, ECM expression and supported a quiescent cell phenotype.

Enzymatic-free passaging

The PLA with thermo-responsive PDEGMA/S-Nor-GGG-YIGSR polymer scaffolds were not only designed to improve cell attachment and phenotype support, but also to prevent cell damage, which can occur through enzymatic passaging. Many studies to date have investigated the potential of the thermo-responsive polymer, PNIPAM, for corneal cell type detachment.[8,35–37] We have recently shown that blend electrospinning of thermo-responsive polymer poly ($PEGMA_{188}$) with a bulk polymer of choice (amenable to electrospinning) will render the fibres thermo-responsive. Mammalian cell adhesion, viability, proliferation and phenotype on this fibrous culture system over numerous thermal enzyme-free passages was achieved.[38] However, no other studies are reported to date utilising such thermo-responsive scaffolds for human primary cell culture. A preliminary experiment illustrating the ability to culture and detach cells from the PLA + PDEGMA and PLA + PDEGMA/S-Nor-GGG-YIGSR-containing scaffolds, and the subsequent quantitative assessment of the cell phenotype by flow cytometry analysis (FACS), was performed. hCSCs grown on peptide-derivatised fibrous scaffolds containing 10 wt% of different molar ratios of PDEGMA/S-pep were passaged after 9 days of cell culture at 37 °C by placing the scaffolds in the fridge for 30 min at 4 °C (section 1 ESI†). Cell detachment was observed from all scaffolds (Fig. 5A). This demonstrates the thermo-responsive passaging capability of the scaffold containing peptide on the surface. However, fluctuating percentages of cells detached were observed from some of the 2 and 10 mol% PDEGS-Nor-GGG-YIGSR (98 : 2, 90 : 10) containing scaffolds (Fig. 5A). This may have been due to heterogeneous

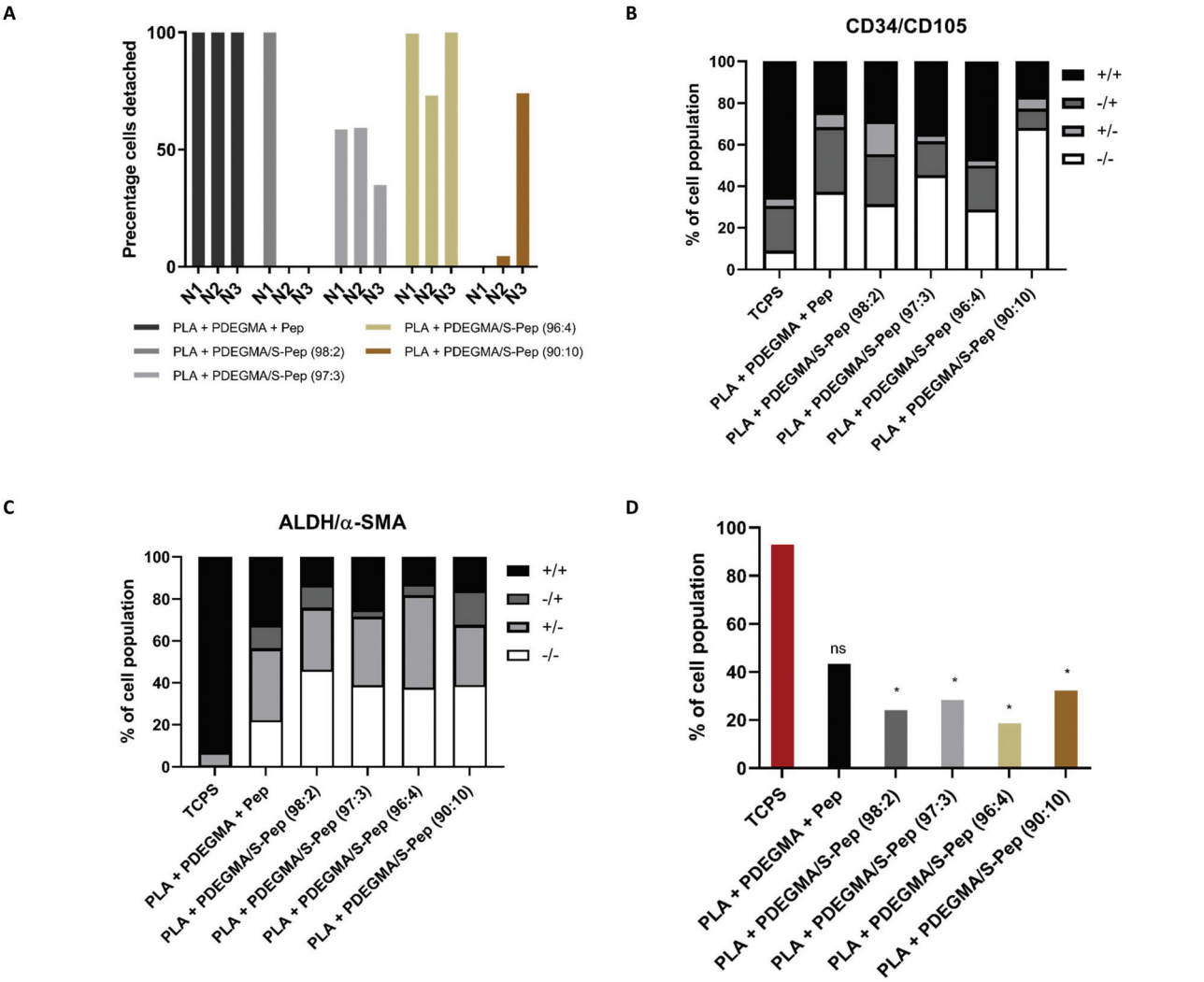

Fig. 5 (A) Percentage of cells detached after thermo-responsive passaging of the different concentrations of peptide on the surface (n = 3 scaffolds, two-way ANOVA, error bars = SD). (B) Flow cytometry percentage of cell population expressing the desired keratocyte marker CD34 and/or mesenchymal stem cell marker CD105 after thermo-response detachment from the different scaffolds (n = 3 cells detached from 3 scaffolds per scaffold type, control cell passage with trypsin from TCPS). (C) Flow cytometry percentage of cell population expressing the desired keratocyte marker ALDH and/or the undesired myo-fibroblastic marker α-SMA after thermo-response detachment from the different scaffolds (n = 3 cells detached from 3 scaffolds per scaffold type, control cell passage with trypsin from TCPS). (D) Combined percentage of cell population that expresses α-SMA on the different scaffolds (n = 3 cells detached from 3 scaffolds per scaffold type, control cell passage with trypsin from TCPS, * = <0.05).

cell attachment to the lowest percentage peptide derivatives (PDEGMA/S-Nor-GGG-YIGSR (98 : 2)) and very strong adhesion to the more extensively peptide-functionalised fibres (PDEGMA/S-Nor-GGG-YIGSR (90 : 10)). Nonetheless, more consistent cell detachment was observed from the scaffolds containing 3 and 4 mol% PDEGS-Nor-GGG-YIGSR (97 : 3 and 96 : 4). The presence of extracellular matrix after detachment was not investigated in this work and will be included in future work.

Flow cytometry analysis of cell surface markers of cells detached from the scaffolds was carried out to validate immuno-staining findings. Cells cultured on 3 mol% peptide scaffolds were observed to have an increased sub-population of 16% of cells that only expressed the $CD34^+/CD105^-$ keratocyte marker (Fig. 5B and Tables S8–9†) compared to those cultured on all other scaffolds. However, $CD34^-/CD105^+$ and $CD34^+/CD105^+$ sub-populations combined constituted half of the total cell population (53%, Table S8†) whereas $CD34^+/CD105^+$ and $CD34^+/CD105^-$ cells comprised 45% (Table S8†) of the total cell population. Therefore, a significant percentage of the population exhibited MSC characteristics besides those of the desired keratocyte CD34 marker. A similar sub-population percentage of $CD34^-/CD105^+$ and $CD34^+/CD105^+$ cells (51%, Table S8†) was detected when cultured on the scaffolds with 4 mol% peptide on the surface, nevertheless there was an increase in the proportion of cells which expressed the CD34 marker (38% of total cell population, Table S8†). Significantly less $CD34^+/CD105^+$ expression was observed for all scaffolds compared to the 2D TCPS control when comparing the Y-mean (Table S9†). This observation

shows that the 3D culture environment significantly reduced the expression of the MSC marker CD105, while no significant difference was seen for the different molar percentage content of peptides (Tables S8 and S10–11†). In addition, an increased expression of $ALDH^+/\alpha\text{-}SMA^-$ was demonstrated when cells were cultured on 3 and 4 mol% peptide scaffolds (Fig. 5C). In terms of the total cell population, 24, 28, 19 and 32% ($ALDH^-/\alpha\text{-}SMA^+$ and $ALDH^+/\alpha\text{-}SMA^+$ combined, Table S8†) for 2, 3, 4 and 10 mol% peptide-functionalised fibres, respectively, were shown to express the α-SMA activated myofibroblastic marker. This was significantly less than the 93% and 43% observed for the 2D control and PLA + PDEGMA scaffold respectively. Hence, the 3D structure of the scaffolds containing covalently bound peptide on the surface reduced the differentiation to the undesired activated myo-fibroblastic phenotype compared to the 2D control. Although no significant difference could be observed between the scaffolds for CD34/CD105 expression, a significant decrease of $ALDH^-/\alpha\text{-}SMA^+$ was seen for the scaffolds with 3 and 4 mol% peptide compared to 2D and the adsorbed peptide scaffold when comparing the X-mean (Tables S8–11†). This gives an indication that the covalently attached peptide reduced the change to the activated myofibroblast phenotype and supported increased ALDH expression.

In general terms, these data were in accord with the improved results in 3D fibrous scaffolds for cell culture and tissue engineering compared to 2D cultures reported in recent years.[39–43] The fibrous structure in these materials was designed to mimic ECM properties, resulting in an increase in desired cell response. However, as the synthetic polymers used in our culture assays were non-native to the cells, we anticipated that peptide or protein incorporation or functionalisation would be required to overcome some key practical challenges. These included poor cell attachment and induction of inflammation or undesired cell differentiation due to the suboptimal mechanical or chemical properties (such as stiffness and hydrophobicity) of conventional polymer fibres.[39–43] For example, Rodina *et al.*[42] investigated migration and proliferation of mesenchymal stromal stem cells (MSSCs) on collagen protein modified PLA fibrous scaffolds. They observed more uniform distribution and cell penetration into these modified scaffolds. In addition to proteins, more specific peptide sequences can be used as ligands for enhanced cell attachment. The Arg-Gly-Asp (RGD) collagen/fibronectin peptide sequence is the most commonly used peptide incorporated in biomaterials to increase their cell adhesion properties.[44] Besides, incorporation of known cell attachment peptide sequences (such as RGD), more cell specific peptide sequences can be incorporated to improve selective cell function or differentiation on the materials.[45] Examples include the laminin-derived peptides IKVAV[46] and YIGSR[47] for cell attachment and anti-cancerous response, specific bone morphogenetic protein-2-related peptide P24 and $rhBMP_2$,[48,49] MMP degradable peptide sequences[50] and enzyme responsive peptides (such as Fmoc-propargyl-GAARGD, which can be cleaved to ARGD by the enzyme elastase expressed by porcine pancreas).[51]

In this study, we set out a new approach for 3D mammalian cell culture by functionalising thermo-responsive fibrous scaffolds with a cell responsive peptide sequence. The methodology employed here to functionalise the scaffolds is amenable to the attachment of other peptide sequences as desired. In our case the laminin-1 peptide component, YIGSR, known to promote hCSCs interaction and to support the quiescent keratocyte culture on the scaffolds was chosen as an exemplar.[22]

Previous studies have demonstrated that laminin improves growth, organisation and differentiation of many cell types.[22,52–55] Nonetheless, the use of laminin has many disadvantages such as degradation in culture to inactive fragments, tumorigenesis and induction of immune-responses, which make the full sequence unsuitable for clinical application.[56] This risk can be minimised by selecting small peptide sequences within the laminin structure, which have the ability to improve adhesion and cell migration. One of these sequences is YIGSR, which has been observed to improve cell adhesion and migration.[57–61] For example, Uzunalli *et al.*[22] investigated the response of hCSCs on bioactive self-assembled peptide nanofibres. Two peptide sequences were investigated; (1) YIGSR (laminin derived) and (2) RGD (fibronectin derived). In both these cases, hCSCs were observed to maintain their characteristic morphology, and their proliferation was enhanced when YIGSR was present. Significantly, less cell proliferation and adhesion was observed for the RGD fibres. This study suggested that the YIGSR sequence has a direct impact on hCSCs attachment, proliferation and migration on 3D structures. These observations are in line with the increase in proliferation of the hCSCs observed on our scaffolds with increasing molar ratio of GGG-YIGSR covalently bound on the surface. Many studies have reported improved attachment and proliferation of human cornea epithelial cells.[61–65] However, only one paper has described the response of hCSCs on YIGSR incorporated scaffolds,[22] and no phenotypic support study has been performed to our knowledge. The immuno-staining and flow cytometry data reported here suggests that not only does YIGSR enhance cell attachment and proliferation on the fibrous scaffold, but the peptide also supports a higher percentage of the cell population which expresses a quiescent phenotype. Down-regulation of the undesired myofibroblastic marker α-SMA was detected, while up-regulation of keratocyte markers CD34 and ALDH was observed. Phenotypic characteristics were observed to remain constant when cultured and passaged, by the thermo-responsive enzymatic free passaging capabilities of the scaffolds. This gives an indication that such scaffolds can be designed to support the desired cell phenotype during *in vitro* culture and enzyme-free passaging and therefore this system is suitable for therapeutically relevant cell types.

Conclusions

The peptide functionalised, thermo-responsive electrospun scaffolds described here were designed for human cornea

stromal cells (hCSCs) proliferation, phenotype support and enzymatic digestion-free passaging. The initially proposed scaffolds (PLA with 10 wt% PDEGMA) did not facilitate hCSCs adhesion and proliferation. Therefore, a peptide-functionalised scaffold was produced to improve the attachment of hCSCs on the scaffold and support the desired quiescent phenotype. PDEGMA/SH polymers were accordingly synthesised, their thermo-responsive properties and thiol content confirmed, and the materials were successfully blend-electrospun with PLA into fibrous scaffolds. The presence and homogenous distribution of free thiol on the scaffold surfaces, and the subsequent conjugation of Nor-GGG-YIGSR was confirmed by ToF-SIMS analysis. Non-specific attachment of the peptide was observed on thermo-responsive fibres without free thiol functionality but microscopy studies showed aggregated cells on these scaffolds, while elongated and spread cell morphologies were observed on thiol-containing and covalently-bound peptide derivatised scaffolds. These data indicated that enhanced hCSCs interaction was dependent on covalent peptide-functionalisation of the thermo-responsive fibres. The undesired, activated myofibroblastic phenotype was observed to decrease with increased molar percentage of Nor-GGG-YIGSR conjugated polymers at the scaffold's surface. The highest levels of peptide-functionalisation resulted in a decrease in keratocyte specific markers ALDH and CD34, whereas concentrations of 3 and 4 mol% Nor-GGG-YIGSR resulted in the highest expression of keratocyte markers, while suppressing the active myofibroblastic phenotype. Between 80–100% of cultured cells were observed to detach from the scaffolds at temperatures below the phase transition temperature of the thermo-responsive polymers at the surfaces of the fibres. Despite some variation in detachment of the cells from the scaffolds, cells were able to retain their cell phenotype after thermal cycles of attachment and detachment passaging. Hence, it can be concluded that the designed peptide conjugated thermo-responsive fibrous scaffolds are suitable for the attachment, proliferation, quiescent keratocyte phenotype support and temperature-mediated-passaging of hCSCs. In our studies, we used a peptide sequence to aid in hCSCs cell culture and expansion, but the attached peptide sequence could easily be changed to select for a different cell type, making the fabricated scaffolds a versatile matrix for cell expansion and phenotype support of any cell type including those destined for the clinic.

Conflicts of interest

There are no conflicts to declare.

Acknowledgements

This work was supported by the Engineering and Physical Sciences Research Council [grant number EP/F500491/1] in the EPSRC Centre of Doctoral Training in Regenerative Medicine. The authors would like to thank Jiang Long and David Scurr for the help in ToF-SIMS and Emily Smith and Marta Alvarez Paino for conducting the XPS measurements and analysis, as well as, Hang Lau, Tianzhi Luo and Michael Haider for their advice and help during the work conducted at the University of Delaware in Prof. Kiick, Prof. Pochan and Dr Martin's labs.

Notes and references

1 K. Duval, H. Grover, L. H. Han, Y. Mou, A. F. Pegoraro, J. Fredberg and Z. Chen, *Physiology*, 2017, **32**, 266–277.
2 R. D. Xu, M. B. Taskin, M. Rubert, D. Seliktar, F. Besenbacher and M. L. Chen, *Sci. Rep.*, 2015, **5**, 8480.
3 C. M. Madl, S. C. Heilshorn and H. M. Blau, *Nature*, 2018, **557**, 335–342.
4 S. Vedicherla and C. T. Buckley, *BioMed Res. Int.*, 2017, **2017**, 2395138.
5 H. L. Huang, H. W. Hsing, T. C. Lai, Y. W. Chen, T. R. Lee, H. T. Chan, P. C. Lyu, C. L. Wu, Y. C. Lu, S. T. Lin, C. W. Lin, C. H. Lai, H. T. Chang, H. C. Chou and H. L. Chan, *J. Biomed. Sci.*, 2010, **17**, 36–46.
6 P. Danhier, T. Copetti, G. De Preter, P. Leveque, O. Feron, B. F. Jordan, P. Sonveaux and B. Gallez, *PLoS One*, 2013, **8**, e53324.
7 F. Gambinossi, L. S. Sefcik, E. Wischerhoff, A. Laschewsky and J. K. Ferri, *ACS Appl. Mater. Interfaces*, 2015, **7**, 2518–2528.
8 S. Nara, S. Chameettachal, S. Midha, H. Singh, R. Tandon, S. Mohanty and S. Ghosh, *J. Mater. Chem. B*, 2015, **3**, 4155–4169.
9 K. Itoga and T. Okano, *J. Mater. Chem.*, 2010, **20**, 8768–8775.
10 S. Dey, B. Kellam, M. R. Alexander, C. Alexander and F. R. A. J. Rose, *J. Mater. Chem.*, 2011, **21**, 6883–6890.
11 X. Xue, L. Thiagarajan, S. Braim, B. R. Saunders, K. M. Shakesheff and C. Alexander, *J. Mater. Chem. B*, 2017, **5**, 4926–4933.
12 A. Saeed, N. Francini, L. White, J. Dixon, T. Gould, H. Rashidi, R. C. Al Ghanami, V. Hruschka, H. Redl, B. R. Saunders, C. Alexander and K. M. Shakesheff, *Adv. Mater.*, 2015, **27**, 662–668.
13 S. A. Braim, K. M. Shakesheff, B. R. Saunders and C. Alexander, *J. Mater. Chem. B*, 2016, **4**, 962–972.
14 J.-F. Lutz, Ö. Akdemir and A. Hoth, *J. Am. Chem. Soc.*, 2006, **128**, 13046–13047.
15 N. Badi, *Prog. Polym. Sci.*, 2017, **66**, 54–79.
16 M. Ulasan, E. Yavuz, E. U. Bagriacik, Y. Cengeloglu and M. S. Yavuz, *J. Biomed. Mater. Res., Part A*, 2015, **103**, 243–251.
17 S. M. Hashemnejad, A. Z. M. Badruddoza, B. Zarket, C. Ricardo Castaneda and P. S. Doyle, *Nat. Commun.*, 2019, **10**, 2749.
18 Y. Yao, Y.-Z. Ma, M. Qin, X.-J. Ma, C. Wang and X.-Z. Feng, *Colloids Surf., B*, 2008, **66**, 233–239.

19 A. M. Aladdad, M. H. Amer, L. Sidney, A. Hopkinson, L. J. White, C. Alexander and F. R. A. J. Rose, *Acta Biomater.*, 2019, **95**, 427–438.
20 C. Zhong, J. Wu, C. A. Reinhart-King and C. C. Chu, *Acta Biomater.*, 2010, **6**, 3908–3918.
21 L. E. Sidney and A. Hopkinson, *J. Tissue Eng. Regener. Med.*, 2018, **12**, e203–e215.
22 G. Uzunalli, Z. Soran, T. S. Erkal, Y. S. Dagdas, E. Dinc, A. M. Hondur, K. Bilgihan, B. Aydin, M. O. Guler and A. B. Tekinay, *Acta Biomater.*, 2014, **10**, 1156–1166.
23 L. E. Sidney, M. J. Branch, H. S. Dua and A. Hopkinson, *Cytotherapy*, 2015, **17**, 1706–1722.
24 K. Hashmani, M. J. Branch, L. E. Sidney, P. S. Dhillon, M. Verma, O. D. McIntosh, A. Hopkinson and H. S. Dua, *Stem Cell Res. Ther.*, 2013, **4**, 226–226.
25 F. A. A. Ruiter, C. Alexander, F. R. A. J. Rose and J. I. Segal, *Biomed. Mater.*, 2017, **12**, 055009.
26 P. Kingshott, S. McArthur, H. Thissen, D. G. Castner and H. J. Griesser, *Biomaterials*, 2002, **23**, 4775–4785.
27 C. M. Mahoney, S. V. Roberson and G. Gillen, *Anal. Chem.*, 2004, **76**, 3199–3207.
28 D. Cossement, R. Gouttebaron, V. Cornet, P. Viville, M. Hecq and R. Lazzaroni, *Appl. Surf. Sci.*, 2006, **252**, 6636–6639.
29 H. K. Shon, M. Son, K. M. Park, C. K. Rhee, N. W. Song, H. M. Park, D. W. Moon and T. G. Lee, *Surf. Interface Anal.*, 2011, **43**, 628–631.
30 Y. Yokoyama, S. Aoyagi, M. Fujii, J. Matsuo, J. S. Fletcher, N. P. Lockyer, J. C. Vickerman, M. K. Passarelli, R. Havelund and M. P. Seah, *Anal. Chem.*, 2016, **88**, 3592–3597.
31 M. Körsgen, A. Pelster, K. Dreisewerd and H. F. Arlinghaus, *J. Am. Soc. Mass Spectrom.*, 2016, **27**, 277–284.
32 S. Ying, A. Shiraishi, C. W. Kao, R. L. Converse, J. L. Funderburgh, J. Swiergiel, M. R. Roth, G. W. Conrad and W. W. Kao, *J. Biol. Chem.*, 1997, **272**, 30306–30313.
33 S. Saika, A. Shiraishi, C. Y. Liu, J. L. Funderburgh, C. W. C. Kao, R. L. Converse and W. W. Kao, *J. Biol. Chem.*, 2000, **275**, 2607–2612.
34 K. Musselmann, B. Alexandrou, B. Kane and J. R. Hassell, *J. Biol. Chem.*, 2005, **280**, 32634–32639.
35 T. Sumide, K. Nishida, M. Yamato, T. Ide, Y. Hayashida, K. Watanabe, J. Yang, C. Kohno, A. Kikuchi, N. Maeda, H. Watanabe, T. Okano and Y. Tano, *FASEB J.*, 2006, **20**, 392–394.
36 J. Teichmann, M. Nitschke, D. Pette, M. Valtink, S. Gramm, F. V. Hartel, T. Noll, R. H. W. Funk, K. Engelmann and C. Werner, *Sci. Technol. Adv. Mater.*, 2015, **16**, 045003–045003.
37 Y.-F. Li, P. Slemming-Adamsen, J. Wang, J. Song, X. Wang, Y. Yu, M. Dong, C. Chen, F. Besenbacher and M. Chen, *J. Tissue Eng. Regener. Med.*, 2017, **11**, 2411–2420.
38 A. M. Aladdad, M. H. Amer, L. Sidney, A. Hopkinson, L. J. White, C. Alexander and F. R. A. J. Rose, *Acta Biomater.*, 2019, **95**, 427–438.
39 N. Masoumi, D. Copper, P. Chen, A. Cubberley, K. Guo, R. Z. Lin, B. Ahmed, D. Martin, E. Aikawa, J. Melero-Martin and J. Mayer, *Adv. Funct. Mater.*, 2017, **27**, 1606614–1606614.
40 J. M. Holzwarth and P. X. Ma, *J. Mater. Chem.*, 2011, **21**, 10243–10251.
41 T. D. Stocco, B. V. M. Rodrigues, F. R. Marciano and A. O. Lobo, *Mater. Lett.*, 2017, **196**, 221–224.
42 A. V. Rodina, T. K. Tenchurin, V. P. Saprykin, A. D. Shepelev, V. G. Mamagulashvili, T. E. Grigor'ev, K. I. Lukanina, A. S. Orekhov, E. Y. Moskaleva and S. N. Chvalun, *Bull. Exp. Biol. Med.*, 2016, **162**, 120–126.
43 J. M. Lee, T. Chae, F. A. Sheikh, H. W. Ju, B. M. Moon, H. J. Park, Y. R. Park and C. H. Park, *Mater. Sci. Eng., C*, 2016, **68**, 758–767.
44 N. J. Hogrebe and K. J. Gooch, *J. Biomed. Mater. Res., Part A*, 2016, **104**, 2356–2368.
45 N. Huettner, T. R. Dargaville and A. Forget, *Trends Biotechnol.*, 2018, **36**, 372–383.
46 A. Farrukh, S. F. Zhao, J. I. Paez, A. Kavyanifar, M. Salierno, A. Cavalie and A. del Campo, *ACS Appl. Mater. Interfaces*, 2018, **10**, 41129–41137.
47 L. M. Nibourg, E. Gelens, S. A. F. Nibourg, M. R. de Jong, R. Kuijer, T. G. van Kooten and S. A. Koopmans, *Acta Ophthalmol.*, 2016, **94**, 721–729.
48 Z. H. Deng, Y. S. Li, X. Gao, G. H. Lei and J. Huard, *Osteoarthritis Cartilage*, 2018, **26**, 1153–1161.
49 J. F. Li, L. Jin, M. B. Wang, S. B. Zhu and S. Y. Xu, *Biomed. Mater.*, 2015, **10**, 045004.
50 J. Yu, F. Chen, X. Wang, N. Dong, C. Lu, G. Yang and Z. Chen, *Polym. Degrad. Stab.*, 2016, **133**, 312–320.
51 J. N. Roberts, J. K. Sahoo, L. E. McNamara, K. V. Burgess, J. L. Yang, E. V. Alakpa, H. J. Anderson, J. Hay, L. A. Turner, S. J. Yarwood, M. Zelzer, R. O. C. Oreffo, R. V. Ulijn and M. J. Dalby, *ACS Nano*, 2016, **10**, 6667–6679.
52 A. M. Baur, T. I. Gamberger, H. G. Weerda, M. Gjuric and E. R. Tamm, *Acta Otolaryngol.*, 1995, **115**, 517–521.
53 K. Stamati, J. V. Priestley, V. Mudera and U. Cheema, *Exp. Cell Res.*, 2014, **327**, 68–77.
54 C. L. Maruyama, N. J. Leigh, J. W. Nelson, A. D. McCall, R. E. Mellas, P. Lei, S. T. Andreadis and O. J. Baker, *J. Dent. Res.*, 2015, **94**, 1610–1617.
55 C. V. Leiton, A. Aranmolate, C. Eyermann, M. J. Menezes, L. F. Escobar-Hoyos, S. Husain, S. J. Winder and H. Colognato, *J. Neurochem.*, 2015, **135**, 522–538.
56 P. Topley, D. C. Jenkins, E. A. Jessup and J. N. Stables, *Br. J. Cancer*, 1993, **67**, 953–958.
57 Y. Hosokawa, Y. Takahashi, Y. Kadoya, S. N. M. Yamashina, Y. Yamada and H. Nogawa, *Dev., Growth Differ.*, 1999, **41**, 207–216.
58 Y. Yamada, K. Hozumi, F. Katagiri, Y. Kikkawa and M. Nomizu, *Biomaterials*, 2013, **34**, 6539–6547.
59 K. Nam, C. S. Wang, C. L. M. Maruyama, P. Lei, S. T. Andreadis and O. J. Baker, *J. Dent. Res.*, 2017, **96**, 798–806.
60 C. Kilic, A. Girotti, J. C. Rodriguez-Cabello and V. Hasirci, *Biomater. Sci.*, 2014, **2**, 318–329.

61 X. D. Duan, C. McLaughlin, M. Griffith and H. Sheardown, *Biomaterials*, 2007, **28**, 78–88.
62 K. Merrett, C. M. Griffith, Y. Deslandes, G. Pleizier and H. Sheardown, *J. Biomater. Sci., Polym. Ed.*, 2001, **12**, 647–671.
63 L. Aucoin, C. M. Griffith, G. Pleizier, Y. Deslandes and H. Sheardown, *J. Biomater. Sci., Polym. Ed.*, 2002, **13**, 447–462.
64 F. Li, D. Carlsson, C. Lohmann, E. Suuronen, S. Vascotto, K. Kobuch, H. Sheardown, R. Munger, M. Nakamura and M. Griffith, *Proc. Natl. Acad. Sci. U. S. A.*, 2003, **100**, 15346–15351.
65 X. Duan and H. Sheardown, *J. Biomater. Sci., Polym. Ed.*, 2007, **18**, 701–711.